

RSC Advances



This is an *Accepted Manuscript*, which has been through the Royal Society of Chemistry peer review process and has been accepted for publication.

Accepted Manuscripts are published online shortly after acceptance, before technical editing, formatting and proof reading. Using this free service, authors can make their results available to the community, in citable form, before we publish the edited article. This *Accepted Manuscript* will be replaced by the edited, formatted and paginated article as soon as this is available.

You can find more information about *Accepted Manuscripts* in the [Information for Authors](#).

Please note that technical editing may introduce minor changes to the text and/or graphics, which may alter content. The journal's standard [Terms & Conditions](#) and the [Ethical guidelines](#) still apply. In no event shall the Royal Society of Chemistry be held responsible for any errors or omissions in this *Accepted Manuscript* or any consequences arising from the use of any information it contains.

ARTICLE

Development of a novel and efficient H₂O₂ sensor by simple modification of screen printed Au electrode with Ru nanoparticle loaded functionalized mesoporous SBA15

Cite this: DOI: 10.1039/x0xx00000x

Received 00th January 2012,
Accepted 00th January 2012

DOI: 10.1039/x0xx00000x

www.rsc.org/

Subhenjit Hazra^a, Hrishikesh Joshi^a, Barun Kumar Ghosh^a, Asif Ahmed^b, Timothy Gibson^b, Paul Millner^b, Narendra Nath Ghosh^{a*}

A novel and efficient electrochemical sensor has been developed to quantitatively measure H₂O₂ concentration by cyclic voltammetry. The sensor was prepared by modifying screen printed gold electrodes by Ruthenium nanoparticle (Ru nanoparticle) loaded thiol functionalized mesoporous SBA15 (Ru@SBA15-SH) which was prepared by three simple steps. During measurement H₂O₂ electrochemically interacted with Ru nanoparticles and was channelled appropriately through the mesoporous structure of SBA15. The developed sensor showed a wide detection range with high sensitivity, durability and reproducibility. Furthermore, a very low limit of detection was reported by the sensor (0.42 μM (~0.0142 ppm)), which was much lower than the permissible exposure limit.

1. Introduction

Detection of hydrogen peroxide (H₂O₂) at a very low concentration level, ppm and below, has become of immense interest to the scientist and technologists. H₂O₂ has plethora of applications in pharmaceutical, clinical, environmental, mining, textile and food manufacturing industries.^{1,2} In many industries very high concentrations of H₂O₂ (greater than 10% w/v) in aqueous solutions are commonly used, which are very oxidizing and corrosive upon contact and cause severe inflammation to various organs of the body such as mucus membranes, gastrointestinal mucosa, skin and eyes.^{3,4} Moreover, in living organisms, besides its well-known cytotoxic effects, H₂O₂ also plays a critical role in regulating diverse biological processes as a signaling molecule in apoptosis, immune cell activation, stomatal closure, vascular remodelling and root growth processes.^{5,6} Formation of H₂O₂ also occurs as a side product from some classic biochemical reactions catalyzed by enzymes such as glucose oxidase (GOx), alcohol oxidase (AOx), lactate oxidase (Lox) cholesterol oxidase (ChoOx), etc.⁷

According to the occupational health and safety administration's norm the permissible exposure limit for inhalation of H₂O₂ vapour is 1 ppm and concentration levels over 7 ppm are known to cause lung irritation.⁸ Therefore, in the academic as well as industrial point of view investigations on H₂O₂ detection are of practical significance. Although, conventional techniques are available for hydrogen peroxide

determination such as titrimetric,⁹ spectrophotometric,¹⁰⁻¹³ deviations in electrical conductivity,¹⁴ fluorometric,¹⁵⁻¹⁷ liquid chromatography,¹⁸ chemiluminescence¹⁹⁻²¹ and electrochemiluminescence²²⁻²³ but they all are complex in nature and in some cases expensive and time consuming. Since H₂O₂ is an electroactive molecule, detection of H₂O₂ by using electrochemistry is the most attractive technique, owing to its cost-effectiveness, portability and instrumental simplicity.²⁴ H₂O₂ can be detected via either oxidation or reduction at solid electrode surfaces. However, the major concern of electrochemistry is its slow kinetics and high over potential. This affects the sensing performance and may incur substantial interference from existing electroactive species, such as ascorbate, urate and bilirubin in real samples. Therefore, in search for an efficient H₂O₂ sensing electrode, a large range of materials, such as redox proteins, dyes, transition metals, metal oxides, metal phthalocyanines, metal porphyrins, redox polymers, carbon nanotubes, mesoporous materials etc, have been employed to detect peroxide over the years.²⁵ Some of the mesoporous materials, such as SBA15, MCM-41 etc. possess a high specific surface area along with high porosity and long range ordering. These materials are often used as supports to host various catalytically active sites since their porous structures enhance the accessibility and mass transportation of the reactant molecules to the active centers.²⁶ These materials have also shown promise to be used in various

sensor applications due to their selectivity and ease of surface functionalization with various reactive groups.²⁴⁻²⁶

Over the years, several nanoparticle based electrochemical sensor have been developed for detection of H₂O₂ where different kinds of electrodes have been used. The glassy carbon (GC) electrode has been widely used in sensor development by modifying the electrode using nanomaterials such as platinum-gold nanoclusters on a graphene sheet,²⁷ Ag nanoparticles²⁸ and cadmium oxide nanoparticles embedded in multiwall carbon nanotubes (MWNT).²⁹ Ferric hexacyanoferrate or Prussian blue (PB) is a well explored compound which catalyses H₂O₂ reduction because of the highly catalytically active reduced form of PB (Prussian white) and also due to the polycrystalline structure of PB.^{30,31} Several reports have suggested the use of prussian blue (PB) modified electrodes coupled with carbon electrodes,³² carbon nanotubes/nanocomposites³³ and even platinum/gold electrodes.³⁴ The major drawback associated with PB is the lack of operational stability in neutral and alkaline solutions because the reduced form of PB, Prussian white, can be dissolved by hydroxide ions.³⁵ Other metal hexacyanoferrates such as Cu, Ni, Co, Cr, V, Ru and Mn hexacyanoferrates can also be used for hydrogen peroxide sensing. These metal hexacyanoferrate based sensors have exhibited a lower capability for electrocatalytic reduction of H₂O₂ than PB based electrodes, but with greater electrochemical stability over a wide range of pH.⁸ Platinum³⁶ and gold electrodes have also been used for sensor applications as both metals increase the response and sensitivity of the electrode.

In the last few years, a huge number of electrochemical devices have been successfully built using screen printing techniques.³⁷ This technology offers multiple advantages including cost effectiveness, flexibility, process automation, reproducibility and usage of variety of materials. Screen printed electrodes can be coupled with the enzyme horseradish peroxidase (HRP) to detect H₂O₂ by using nanoparticles in chitosan matrix,³⁸ labelling Au colloids immobilized on a gold electrode via a cysteamine monolayer with HRP³⁹ or even by direct electron transfer between the screen printed electrode and HRP.^{40,41} Ruthenium complexes (such as K[Ru(EDTA-H)C1].2H₂O,⁴² Ru(III)phosphate⁴³) were used in developing electrochemical sensors for H₂O₂, as these complexes could effectively perform electron transfer reaction with peroxide.⁴⁴ Ruthenium(IV) oxide has also been known to interact with H₂O₂, and was used to study catalysis activity in plants.⁴⁵ Apparently, the Ru hcp crystal structure of the nanoparticles adsorbs OH_{ads} as well as O_{ads} readily, and hence, can successfully catalyze the H₂O₂ degradation in electrochemical system.⁴⁶ However, the electrochemical sensors developed and reported until now, involve complex preparation protocols and suffers from poor response and sensitivity. Moreover, the sensors developed using HRP require specific conditions of pH, buffer and optimal temperature for effective detection and reproducibility. Furthermore, in many of the reported sensors the preparation method for the nanomaterials are quite complex.

In the present investigation, we have adopted a strategy to construct a composite material by immobilizing metal nanoparticles (here Ru nanoparticle) within the porous structure of mesoporous silica (SBA15) so that we can exploit both the advantages offered by nanoparticle as well as mesoporous silica. The preparation of these nanoparticles involves two simple post treatments of SBA15. In the first step Ru nanoparticles were incorporated in the silica matrix and second step involved thiol functionalization of the Ru nanoparticle incorporated SBA15. After functionalization of Ru@SBA15, the nanocomposites (Ru@SBA15-SH) were attached to the surface of screen printed Au electrodes by a simple drop cast technique. We modified the screen printed gold electrode (SPE) as it serves as a good and cost effective mediator for electron transfer. The synthesized material was characterized by BET, XRD, FTIR and electron microscopy.

Here, we report development of an efficient, sensitive and robust hydrogen peroxide sensor with a simple preparation technique. The functionalized materials were easily deposited on the gold electrodes as the thiol groups present on surface interacted effectively with the gold surface. A thorough electrochemical study was conducted to establish linearity and sensitivity of current response, reliability of sensor, durability of electrode and also to determine the limit of detection.

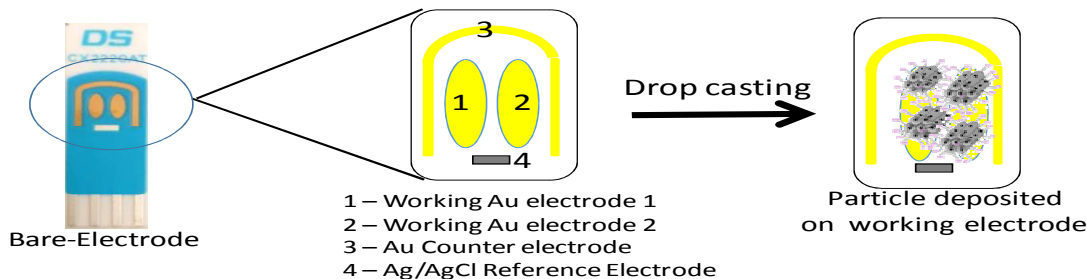
2. Experimental Section

2.1 Materials

Tetraethyl orthosilicate (TEOS), conc. Hydrochloric acid (HCl), EO₂₀PO₇₀EO₂₀ (P123), Ruthenium chloride hydrate (RuCl₃. xH₂O), and Toluene were purchased from Merck, India. Custom made screen-printed gold electrodes (circular working electrodes, CX2223AT) were supplied by Drop Sens S.L. (Oviedo, Spain). These electrodes consist of ceramic base with Ag/AgCl reference and Au counter electrode on same chip. H₂O₂ (30% w/v solution) and (3-mercaptopropyl)trimethoxysilane (MPTMS) were purchased from Sigma Aldrich. Deionized water and 0.1 M PBS buffer, pH of 7.0 were used throughout the experiments.

2.2 Synthesis of SBA15 (SBA15)

Mesoporous silicate SBA15 was synthesized using a liquid crystal templating method using Pluronic P123, tetraethyl orthosilicate and concentrated hydrochloric acid.⁴⁷ In a typical synthesis of SBA15, 3.3 g of Pluronic P123 was dissolved in 101 g of water with 8 g of concentrated hydrochloric acid. The mixture was stirred until the formation of a clear solution. Then, 6.93 g of tetraethyl orthosilicate was added to this solution and stirred for 4 h. The resulting mixture was then transferred to a Teflon bottle and heated at 90 °C for 24 h to allow condensation. The precursor formed was then filtered and washed with 150 mL of distilled water and dried in the oven at 100 °C. It was then calcined at 550 °C for 3 h in an air atmosphere to obtain SBA15.

Step 1: Preparation of Ru@SBA15-SH**Step 2: Depositing Ru@SBA15-SH on the working electrode**

Scheme 1: Schematic representation of preparation of Ru@SBA15-SH based sensor

2.3 Synthesis of Ruthenium nanoparticle incorporated SBA15 (Ru@SBA15)

Ru nanoparticle loaded SBA15 samples (10 % w/w Ru) were synthesized. Here, $\text{RuCl}_3 \cdot x\text{H}_2\text{O}$ was reduced by sodium borohydride (NaBH_4) using a molar ratio of $\text{RuCl}_3 \cdot x\text{H}_2\text{O} : \text{NaBH}_4$ of 1:5. In a typical synthesis, 450 mg of SBA15 was soaked overnight with 125 mg $\text{RuCl}_3 \cdot x\text{H}_2\text{O}$ in 12 ml of water. To this mixture 340 mg of NaBH_4 dissolved in 10 ml of water was slowly added and stirred for 8 h. Finally, the solution was filtered using Whatman-41 filter paper and product was vacuum dried.

2.4 Synthesis of thiol functionalized Ru@SBA15 (Ru@SBA15-SH)

The synthesized Ru@SBA15 was thiol functionalized using (3-mercaptopropyl)trimethoxysilane (MPTMS). Here, 100 mg of Ru@SBA15 was dispersed in 10 ml of dry toluene and 500 μl of MPTMS was added to it. The reaction mixture was then refluxed under a nitrogen atmosphere for 8 h. Then the thiol functionalised Ru@SBA15 was filtered using Whatman-41 filter paper and thoroughly washed with dry toluene to remove excess MPTMS. Finally synthesized particles were dried under vacuum. After thiol functionalization, 1g Ru@SBA15 resulted in the formation of 1.4 g Ru@SBA15-SH. A similar synthesis procedure was followed to synthesize a control material designated as SBA15-SH by using pure SBA15 instead of Ru@SBA15 to study the effect of Ru nanoparticle on peroxide detection.

2.5 Electrode preparation

The electrode surface was cleaned by washing the surface with deionized water. 1 mg of thiol functionalized Ruthenium embedded SBA15 (Ru@SBA15-SH) was dissolved in 100 μl of deionized water and sonicated for 5min. $\sim 5\mu\text{l}$ of the solution was deposited onto the gold surface of the electrode and kept in a moist atmosphere for 4 h to immobilize the particles on the surface. The electrode was then gently washed with a stream of deionized water and then dried by gently blowing nitrogen over

it. The overall protocol for the preparation of the electrode is given in Scheme 1. A control electrode was also prepared by a similar procedure but by using SBA-SH instead of Ru@SBA15-SH.

2.6 Characterization

Thermogravimetric analysis (TGA) was carried out for Ru@SBA15 and Ru@SBA15-SH using a DTG-60 (Shimadzu, Japan) in an air flow at a heating rate of 10 $^\circ\text{C}/\text{min}$ between 30 $^\circ\text{C}$ to 800 $^\circ\text{C}$. Platinum sample pans were used for TGA. Room temperature X-ray diffraction spectra of the samples were recorded by using a powder X-ray diffractometer (Mini Flex II, Rigaku, Japan) with $\text{Cu K}\alpha$ ($\lambda = 0.15405 \text{ nm}$) radiation. Transmission electron microscopic (HRTEM) (JEOL JEM 1400, Japan) images of samples were used to analyze the pores and size of the synthesized nanoparticles. The morphology of the nanoparticles, deposited on the electrode surface, was studied using scanning electron microscopy (SEM) (JSM-6360LV, JEOL, Japan) using an accelerating voltage of 15 kV. Energy-dispersive X-ray spectroscopy (EDS) spectra was recorded using JEOL JSM-5800LV scanning microscopy (JEOL, Japan). Nitrogen adsorption-desorption isotherms, surface area, pore diameter, pore volume were obtained with a surface area and porosity analyzer (Micromeritics Tristar 3000, USA). FTIR spectroscopy was carried out using FTIR-IR infinity-101660, (Shimadzu, Japan). All of the samples were milled with spectroscopic grade potassium bromide (KBr, Merck), and the pellet of mixture was pressed into a disc and placed in solid cell and scanned in the range 4000–400 cm^{-1} . Electrochemical studies were performed using Eco Chemie B V Autolab electrochemical workstation using GPES software for cyclic voltammetry study and FRA software for the impedance study. All electrochemical experiments were performed in open air condition. We have reported here the highly reproducible cyclic voltammogram which is average of two successive measurements. The limit of detection (LOD) was calculated as

$3S_a/b$ where S_a denotes the standard deviation of the intercept and b is the slope for the linear fit ($[I-I_0] = a + b[H_2O_2]$) where I_0 is current value at $[H_2O_2] = 0$ and Signal/Noise ratio is 3.⁴⁸⁻⁵¹

3. Results and Discussion

3.1 Physical characterization of Materials

X-ray diffractograms of the synthesized materials, e.g. SBA15, Ru@SBA15 and Ru@SBA15-SH are shown in Fig. 1. In the XRD patterns for Ru@SBA15 and Ru@SBA15-SH samples, diffraction peak at $2\theta=43.42^\circ$ corresponding to (101) diffraction plane of hcp Ru [JCPDS card no. 65-1863] was observed along with the broad peak of SBA15. XRD patterns of Ru@SBA15 and Ru@SBA15-SH also showed diffraction peaks at $2\theta=38.38^\circ, 58.3^\circ, 69.44^\circ, 78.38^\circ$ corresponding to (100), (102),

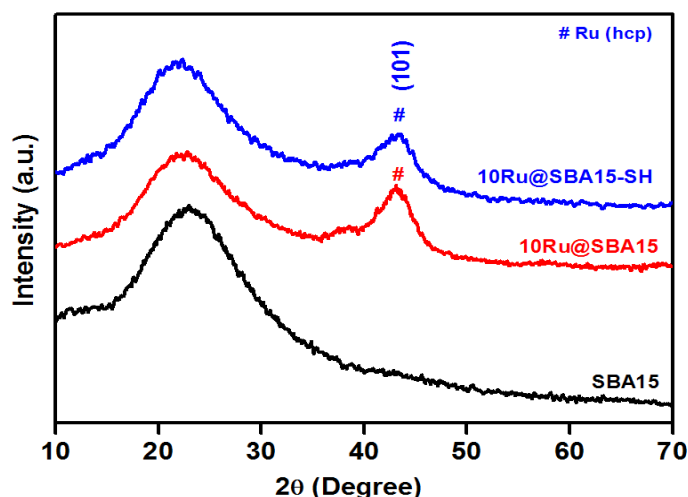


Fig. 1: Wide angle XRD spectra of SBA15, Ru@SBA15 and Ru@SBA15-SH.

(110), and (103) diffraction planes of hcp Ru [JCPDS card no. 65-1863] (Fig. S1 (A) and (B)).^{52,53,54} However, these peaks were found to be very weak, because of the fact that Ru nanoparticles are embedded within the porous matrix of SBA15. Crystallite size of Ru nanoparticles was calculated using Scherrer's equation and was found to be ~ 8 nm.

TG analysis of Ru@SBA15 and Ru@SBA15-SH confirmed the functionalization of SBA15 by MPTMS (Fig. 2). In the

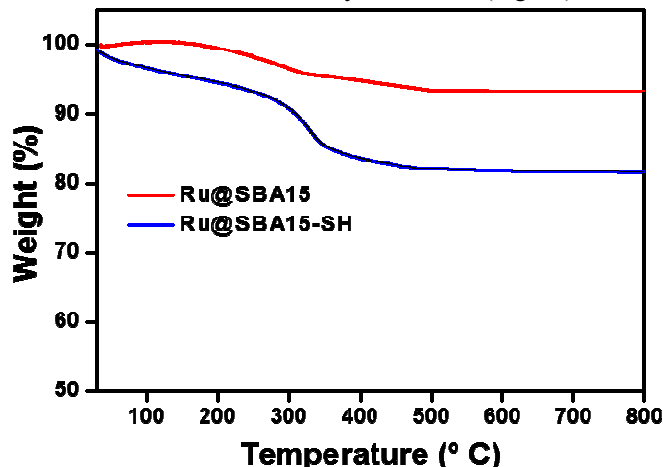


Fig. 2: TGA thermogram of Ru@SBA15-SH and Ru@SBA15.

thermogram of Ru@SBA15-SH, $\sim 15\%$ weight loss was observed in the temperature range 150-550 $^\circ\text{C}$, whereas no significant weight loss was observed in the case of Ru@SBA15. This weight loss might be due to the oxidative thermal decomposition of MPTMS which was present in Ru@SBA15-SH. This weight loss also indicated that, during thiol functionalization ~ 0.33 mole MPTMS is attached with 1 mole of SBA15, which matches with the theoretically calculated amount of thiol functionalization in Ru@SBA15-SH (refer section 2.4)

FTIR spectra of Ru@SBA15 and Ru@SBA15-SH are shown in Fig. 3, which confirmed the thiol functionalization of the material. The broad intense peak at 3500-3300 cm^{-1} in Ru@SBA15 was assigned to the Si-OH group of SBA15. The

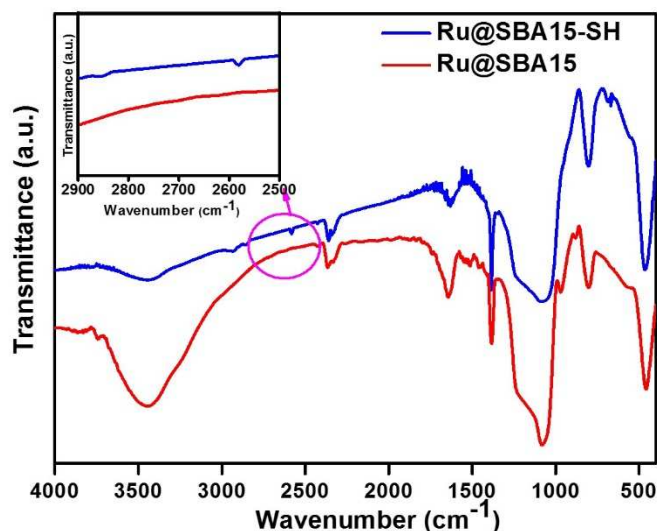


Fig. 3: FTIR spectra of Ru@SBA15-SH and Ru@SBA15. Inset graph : FTIR spectra showing -SH peak.

intensity of this peak was found to be significantly decreased when Ru@SBA15 was functionalized by MPTMS to prepare Ru@SBA15-SH. This fact indicated the reaction of Si-OH of Ru@SBA15 with $-\text{Si}(\text{OMe})_3$ group of MPTMS. FTIR spectra of Ru@SBA15 also showed the presence of peaks at 2574 cm^{-1} and 2956 cm^{-1} which are characteristic peaks of -SH group and -CH of propyl group MPTMS.

N_2 adsorption-desorption analysis of pure SBA15 and Ru@SBA15 (Fig. 4) showed type IV isotherms with a H1 hysteresis loop, which is characteristic of mesoporous material having a regular pore structure. However, the BET surface area was found to be decreased due to the 10% (w/w) Ru nanoparticle loading in Ru@SBA15. It was also observed that the upper closure point of the hysteresis loop of Ru@SBA15 (at $P/P_0 = 0.95$) appeared at a relatively higher value than that of pure SBA15 (at $P/P_0 = 0.78$). This fact indicates that formation of Ru nanoparticles within the pores of SBA15 blocked some of the channels and caused partial strain and distortion in the pores. Pore volume was also found to be decreased from 1.01

m^3/g to $0.76 \text{ m}^3/\text{g}$ due to Ru nanoparticle loading into the SBA15 matrix.

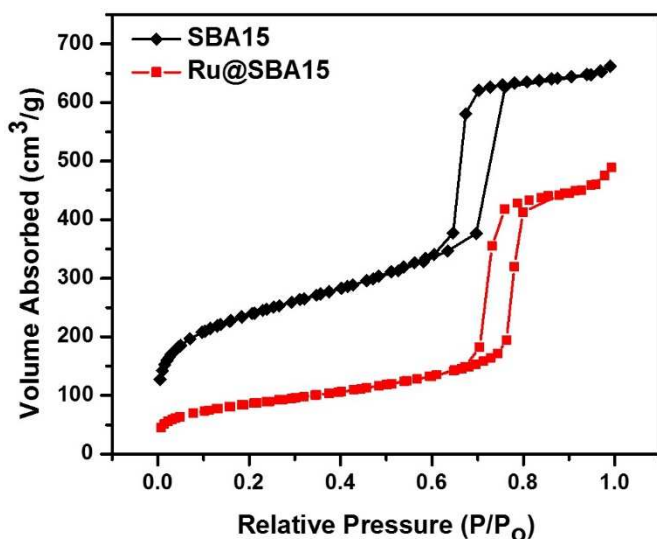


Fig. 4: N_2 adsorption and desorption isotherm of SBA15 and Ru@SBA15.

TEM micrographs of the synthesized materials are shown in Fig. 5(a-d). Regular hexagonal porous structure with long range ordering and long channels with pore diameters of 7-10 nm were observed for pure SBA15. Ru loaded samples, i.e.

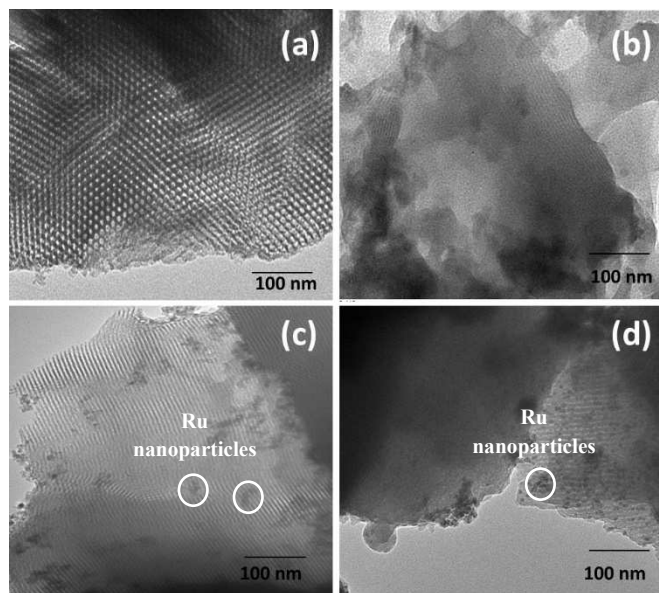


Fig. 5: TEM micrographs of (a) Pure SBA15, (b) SBA-SH, (c) Ru@SBA15 and (d) Ru@SBA15-SH.

Ru@SBA15 and Ru@SBA15-SH, showed the presence of uniform spherical shaped Ru nanoparticles ($\sim 8 \text{ nm}$) within and on the surface of the porous matrix of SBA15. EDS analysis of the samples also confirmed the presence of Ru in Ru@SBA15 (Fig. S2). Another important observation is that even after Ru loading as well thiol functionalization of

Ru@SBA15 the porous nature of SBA15 long channels remained intact. The highly porous and regular ordered structure of Ru@SBA15 should enhance rapid electron transfer to enzyme active sites during electrochemical analysis.

Surface morphology of bare Au electrode and electrode surface after deposition of Ru@SBA15-SH and SBA15-SH was investigated by SEM (Fig. 6 (a), (b)). The micrographs revealed the relatively smooth surface of the bare electrode before deposition of Ru@SBA15-SH.

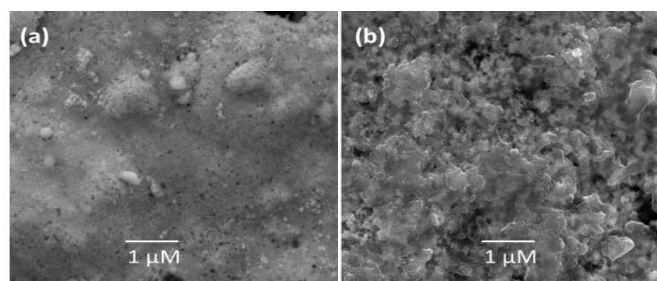


Fig. 6: SEM micrographs of (a) Bare electrode, (b) Ru@SBA15-SH deposited electrode.

3.2 Electrochemical studies

Electrochemical impedance spectroscopy (EIS) yields substantial information about the modifications on the electrode surface. Fig. 7 shows the impedance data of bare Au electrode, control electrode (SBA15-SH deposited on Au SPE), sensor electrode (Ru@SBA15-SH deposited on Au SPE) in 10mM (1:1 ratio) $[\text{Fe}(\text{CN})_6]^{3-/4-}$. The higher R_{ct} values of sensor and control electrodes than the bare electrode (in Nyquist plots) clearly indicate the deposition of particles on both (control and sensor) electrodes. The equivalent circuit of the electrochemical system⁵⁵ is given in Fig. 7. High R_{ct} value of the sensor electrode can be accounted for by the fact that mesoporous channels in SBA15 have been blocked by the Ru nanoparticles, thereby reducing the accessibility of the gold surface for direct

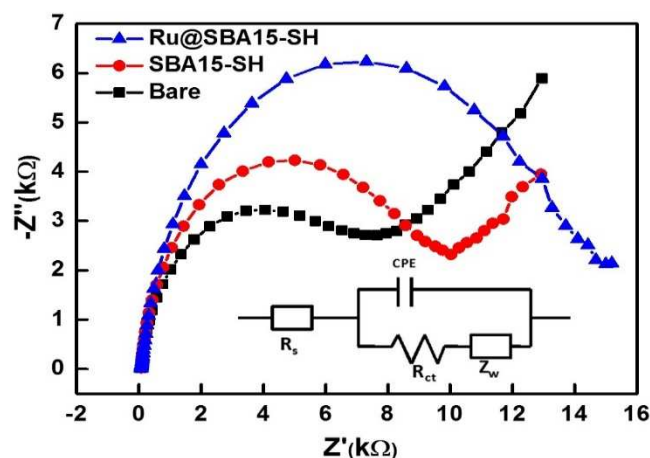


Fig. 7: Nyquist plots of bare electrode, SBA15-SH deposited on electrode and Ru@SBA15-SH deposited on electrode. Inset picture: Equivalent electrochemical circuit.

electron charge transfer. Also the cyclic voltammogram of the sensor (Fig. 8) showed a large deviation in oxidation and reduction potential whereas the control sensor shows almost no deviation proving that incorporated Ru nanoparticles caused the deviations in the electrochemical properties. As Ru is electrochemically very active, hence due to the electrochemical interaction between ferri-ferrocyanide and Ru nanoparticles, which are present in sensor electrode (i.e. Ru@SBA15-SH modified Au electrode), the cyclic voltammetry showed higher peak for Ru@SBA15-SH deposited Au electrode (sensor electrode) in comparison with SBA15-SH modified Au electrode (control electrode) and bare Au electrode (Ru nanoparticles were not present in control electrode and bare electrode).

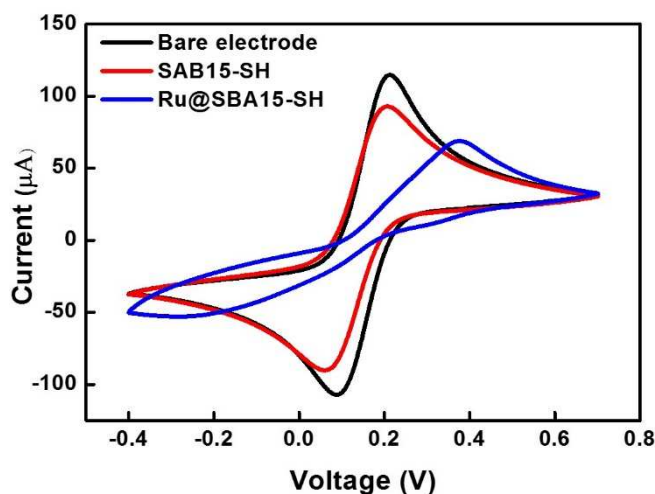


Fig. 8: Cyclic voltammogram of bare electrode, SBA15-SH deposited on electrode and Ru@SBA15-SH deposited on the electrode.

Ru has been known to be involved in various redox couple reactions with H_2O_2 ,^{56,57} hence the Ru nanoparticles are expected to be involved in the charge transfer to detect peroxide quantitatively. To conduct quantitative measurement of H_2O_2 the potential range was set from -0.4 V to 0.75 V in 0.1 M PBS. Potential scan from -0.6 V to 1.5 V was also carried out,

however, in the cyclic voltammogram extra peaks for oxidation were appeared after 1 V (Fig. S3(A)). Moreover, formation of some bubbles near the electrode surface was observed when scan was conducted from -0.6 V to 1.5 V. This might be due to the oxidation of the Au electrode surface. Reproducibility of the results was also reduced when scans were conducted with this high potential range (Fig. S3(B)). The nature of the voltammogram was also altered after the high potential scan (Fig. S3(B)). Therefore, the potential range from -0.4 V to 0.75 V was set all the measurements. Fig. 9(A) shows a cyclic voltammogram in 0.1 M PBS (pH 7) with increasing concentrations of H_2O_2 onto the sensor electrode. It was observed that current at 0.75 V is directly proportional to the concentration of H_2O_2 . Fig. 9(B) suggests that such an enhanced current response is absent in the case of bare and control electrodes, thereby proving that only Ru nanoparticles when interacted with H_2O_2 generate enhanced response. There have been reports demonstrating the use of only gold electrodes to sense H_2O_2 ; but the reported current signal is almost 60 times lower than this sensor.³⁰ The range of detection for H_2O_2 of this Ru@SBA15-SH modified SPE sensor is shown in Fig. 10. This sensor showed a linear trend over the mM as well as μ M

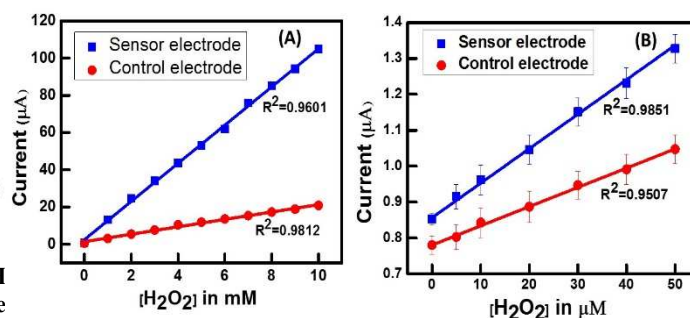


Fig. 10: Current value at (V=0.75V) vs concentration over (A) mM range and (B) μ M range.

concentration ranges. The linear trend was also followed by the control and bare electrodes but with a much less current. It is suspected that this was due to charge transfer between the gold electrode and peroxide.³ There was not much difference in current values between bare and control electrodes (Fig. 9(B)) which signifies that the deposited silica particles caused almost no change to the electrochemical system. Hence, in case of the sensor Ru nanoparticles were responsible for the enhanced current values. The highest current value appeared at the oxidation peak which supports the mechanism of the charge transfer between peroxide and Ru nanoparticles. Peroxide oxidizes Ru nanoparticles to Ru^{III} which occurs at a potential of 0.75 V (pH 7 solution). The linearity of the sensor ranged from 2×10^{-6} M to 10^{-1} M. Above this concentration the peroxide solution became highly corrosive and prolonged exposure of the electrode in the solution degraded the surface of the sensor. Sensitivity of the current response for the developed sensor was $11.26 \mu A mM^{-1}$ calculated using an average of $n=10$ signals each having a triplicate reading.

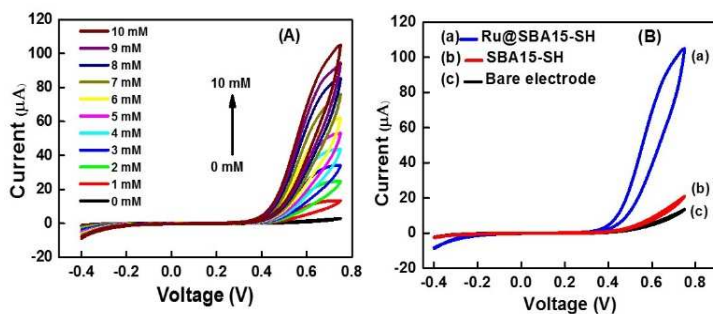


Fig. 9: (A) Cyclic voltammograms of Ru@SBA15-SH electrode with varying concentration of H_2O_2 , (B) Cyclic voltammogram of (a) Ru@SBA15-SH, (b) SBA15-SH modified electrode and (c) bare electrode with $[H_2O_2] = 10$ mM.

Fig. 11(A) shows a cyclic voltammogram of three electrodes (prepared by the same process) in 0.1 M PBS and interrogated with 10 mM H₂O₂. It was very clear that the current values were quite reproducible with no more than 6.2% relative standard deviations. Fig. 11(B) shows a plot of an electrode prepared on day 1 and tested with 10 mM and 5 mM of H₂O₂ on day 31 (~1 month apart). The plot shows almost similar response on both the days for 5 mM as well as 10 mM which

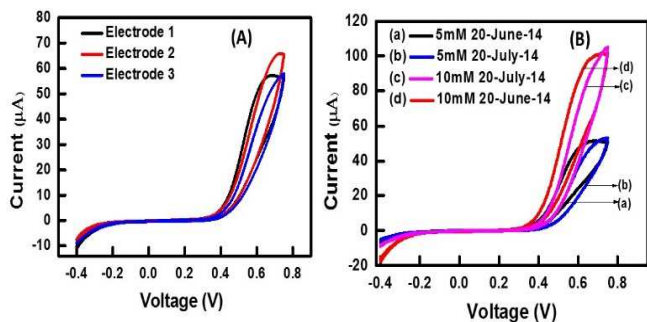


Fig. 11: (A) CV for 3 electrodes with 5 mM H₂O₂. (B) CV of one electrode tested at 5 mM and 10 mM H₂O₂ after storage.

indicates the durability of the sensor. The sensor was stored at room temperature in an airtight box.

Limit of detection (LOD) for a sensor is an important

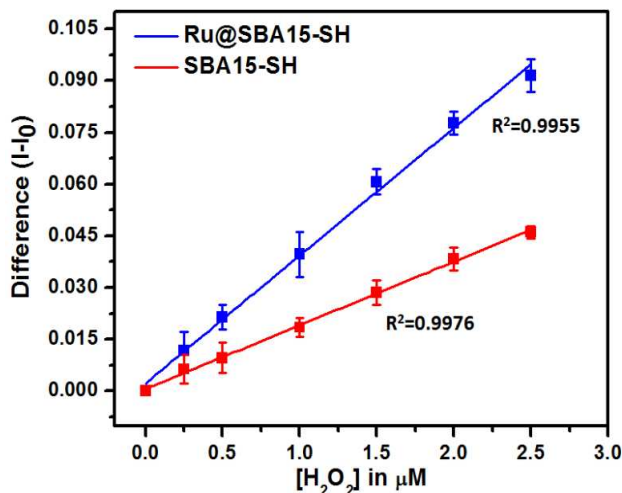


Fig. 12: Limit of detection of the sensor (Ru@SBA15-SH deposited on Au SPE).

characteristic. To determine the limit of detection, the difference in current values (I-I₀) were plotted for the sensor (blue line) as well as control (red line) electrode. The Standard deviation for each data point was computed by using current values obtained from 3 different electrodes prepared by the same procedure as described in the experimental section. The standard deviation and respective mean values were plotted and fitted by a linear curve for both sensor as well as control. The correlation coefficients of the fitted line for sensor and control were 0.9955 and 0.9976 respectively. The limit of detection

was found to be 4.22×10^{-7} M (~0.0143 ppm) (based on Signal/Noise= 3)⁴⁸⁻⁵¹. Also the standard deviations of control and sensor at the point closest to limit of detection (0.4 μM) were well separated, supporting this LOD value.

Conclusions

Here, we have reported the preparation of Ru@SBA15-SH modified screen printed Au electrode for quantitative measurement of H₂O₂ concentration in aqueous medium. This sensor shows its capability to measure wide range of concentration of H₂O₂ (from 100 mM to 2 μM) reliably with high sensitivity. The detection limit of this sensor is as low as $\sim 4.22 \times 10^{-7}$ M, which is well below the permitted standards of H₂O₂. To the best of our knowledge, the LOD for the sensor reported here is lowest among most of the reported electrochemical sensors for H₂O₂ detection. Table 1 listed the LOD values of some of the electrochemical sensors for detection of H₂O₂. High sensitivity, wide range of detection, good durability, reliability and high efficiency make this electrode an attractive sensor for quantitative detection of H₂O₂. This electrode, with some modification has also shown promising results for detection of glucose, lactose and alcohol and the results will be communicated shortly.

Table 1: Comparison of various H₂O₂ electrochemical sensors developed using different materials.

Sr no.	Material used	Detection Method	LOD (μM)	Ref
1.	Pt/Au gold disk	CV / Amperometry	4.00	30
2.	Ru(bpy) ₃ ²⁺ - RuO ₂ .xH ₂ O	Fluorescence-optical sensor	100	45
3.	Pt-Ru Bimetallic nanoparticle	Amperometry	10	46
4.	CPE-RuNP	Amperometry	3.78×10^6	51
5.	Ag nanoparticle	Amperometry	0.6	58
6.	Ag-DNA hybrid NPs	Amperometry/CV	0.6	59
7.	Au NP-TiO ₂ Nanotube	CV / Chronoamperometry	2.00	60
8.	HRP-graphene	Electrochemistry	1.17	61
9.	HRP-Au nanoparticle	Electrochemistry	5.90	62
10.	TiO ₂ nanotube array	Amperometry	1.2	63
11.	Co ₃ O ₄ nanowires	Electrochemistry	1.4	64
12.	Ru@SBA15-SH on Au SPE	CV	0.4	This sensor

Acknowledgements

Dr. N. N. Ghosh and Prof. P. A. Millner gratefully acknowledge financial support from DST-UKIERI. The authors would like to thank Mr. Areef Sardar, NIO, Goa for providing EDS measurements.

Notes and references

Corresponding author. Tel./fax: +91 832 2580318/2557033. E-mail address: naren70@yahoo.com (N. N. Ghosh).

^a Nano-Materials Lab, Department of Chemistry, Birla Institute of Technology and Science, Pilani K. K. Birla Goa Campus, Zuarinagar, Goa 403726, India.

^b School of Biomedical Sciences, Faculty of Biological Sciences, University of Leeds, Leeds, United Kingdom.

Electronic Supplementary Information (ESI) available: Wide angle XRD spectrum of Ru@SBA15 and Ru@SBA15-SH, EDS spectra of Ru@SBA15, and cyclic voltammogram for High Potential range Scan (HPS). See DOI: 10.1039/b000000x

- C. G. Tsiafoulis, P. N. Trikalitis and M. I. Prodromidis, *Electrochem. Commun.*, 2005, **7**, 1398.
- V. Biju, *Chem. Soc. Rev.*, 2014, **43**, 737.
- C. Laloi, K. Apel, A. Danon and C. Opín, *Plant Biology*, 2004, **7**, 323.
- W. Chen, S. Cai, Q. Ren, W. Wen and Y. Zhao, *Analyst*, 2010, **137**, 49.
- Y. Fujita, K. Wakabayashi, M. Nagao and T. Sugimura, *Mutat. Res. Lett.*, 1985, **144**, 227.
- L. Vitetta and A. W. Linnane, *J Inflammopharmacology*, 2014, **22**, 69.
- M. Giorgio, M. Trinei, E. Migliaccio and P. G. Pelicci, *Nature Rev. Mol. Cell Biol.*, 2007, **8**, 722.
- A. Mills, C. Tommons, R. T. Bailey, M. C. Tedford and P. J. Crilly, *Analyst*, 2007, **132**, 566.
- W. H. McCurdy Jr. and H. F. Bell, *Talanta*, 1966, **13**, 925.
- K. Zhang, L. Mao and R. Cai, *Talanta*, 2000, **51**, 179.
- M. C. O. R. F. P. Nogueira and W. C. Paterlini, *Talanta*, 2005, **66**, 86.
- M. Hoshino, S. Kamino, M. Doi, S. Takada, S. Mitani, R. Yanagihara, M. Asano, T. Yamaguchi and Y. Fujita, *Spectrochim. Acta A*, 2014, **117**, 814.
- Q. Chang, K. Deng, L. Zhu, G. Jiang, C. Yu and H. Tang, *Microchim. Acta*, 2009, **165**, 299.
- Y. Yang, Q. Li, X. Yu, X. Chen and Y. Wang, *Food Control*, 2014, **39**, 198.
- M. Schäferling, D. B. M. Grögel and S. Schreml, *Microchim. Acta*, 2011, **174**, 1.
- S. G. Rhee, T. Chang, W. Jeong and D. Kang, *Mol. Cell.*, 2010, **29**, 539.
- X. Chen, D. Li, H. Yang, Q. Zhu, H. Zheng and J. Xu, *Anal. Chim. Acta*, 2001, **434**, 51.
- T. Huang, M. E. Garceau and P. Gao, *J. Pharm. Biomed. Anal.*, 2003, **31**, 1203.
- S. Hanaoka, J. Lin and M. Yamada, *Anal. Chim. Acta*, 2001, **426**, 57.
- A. Tahirović, A. Čopra, E. Omanović-Miklićanin and K. Kalcher, *Talanta*, 2007, **72**, 1378.
- L. Zhang, Y. Chen, Z. Zhang and C. Lu, *Sensor Actuat. B-Chem*, 2014, **193**, 752.
- X. Hu, H. Han, L. Hua and Z. Sheng, *Biosens. Bioelectron.*, 2010, **25**, 1843.
- M. Xu, W. Qi, L. Zhang, J. Lai, A. Rehman, S. Majeed and G. Xu, *Microchim. Acta*, 2014, **181**, 737.
- A. Chen and S. Chatterjee, *Chem. Soc. Rev.*, 2013, **42**, 5425.
- M. Holzinger, A. L. Goff and S. Cosnier, *Front. Chem.*, 2014, **2**, 2296.
- J. Wang, *Analyst*, 2005, **4**, 421.
- X. Cui, S. Wu, Y. Li and G. Wan, *Microchim. Acta*, 2015, **182**, 265.
- K. Cui, Y. Song, Y. Yao, Z. Huang and L. Wang, *Electrochem. Commun.*, 2008, **10**, 663.
- N. Butwong, L. Zhou, W. Ng-eontae, R. Burakham, E. Moore, S. Srijaranai, J. H.T. Luong and J. D. Glennon, *J. Electroanal. Chem.*, 2014, **717**, 41.
- A. A. Karyakin, E. E. Karyakina and Lo Gorton, *Anal. Chem.*, 2000, **72**, 1720.
- A. A. Karyakin, *Electroanalysis*, 2001, **13**, 813.
- N. A. Hirst, L. D. Hazelwood, D. G. Jayne and P. A. Millner, *Sensor Actuat. B-Chem*, 2013, **186**, 674.
- E. Nossola and A. J. G. Zabin, *J. Mater. Chem.*, 2012, **22**, 1824.
- I. L. Mattos, L. Gorton, T. Ruzgas, *Biosens. Bioelectron.*, 2003, **18**, 193.
- U. Scharf and E. W. Grabner, *Electrochim. Acta*, 1996, **41**, 233.
- Y. Zhang and G. S. Wilson, *J. Electroanal. Chem.*, 1993, **345**, 253.
- T. Tangkuaram, C. Ponchio, T. Kangkasomboon, P. Katikawong and W. Veerasai, *Biosens. Bioelectron.*, 2007, **22**, 2071.
- C. Gao, Z. Gao, J. Liu and X. Huang, *Nanoscale*, 2012, **4**, 1948.
- Y. Xiao, H. Ju and H. Chen, *Anal. Chim. Acta*, 1999, **391**, 73.
- X. Xu, S. Liu and H. Ju, *Sensors*, 2003, **3**, 350.
- S. Ledru, N. Ruillé and M. Boujtita, *Biosens. Bioelectron.*, 2006, **21**, 1591.
- M. M. T. Khan, A. Hussain, G. Ramachandraiah and M. A. Moiz, *Inorg. Chem.*, 1986, **25**, 3023.
- P. Li, H. Liu, J. Yang, D. Sun, Y. Chen, Y. Zhou, C. Caia and T. Lua, *J. Mater. Chem. B*, 2014, **2**, 102.
- C. A. Marquette and L. J. Blum, *Anal. Bioanal. Chem.*, 2008, **390**, 155.
- M. F. Dousikou, M. A. Koupparis and C. E. Efsthathiou, *Phytochem. Anal.*, 2006, **17**, 255.
- M. Janyasupab, Y. Zhang, P. Lin, B. Bartling, J. Xu and C. Liu, *J. Nanotech.*, 2011, DOI: 10.1155/2011/506862.
- D. Zhao, J. Feng, Q. Huo, N. Melosh, G. H. Fredrickson, B. F. Chmelka and G. D. Stucky, *Science*, 1998, **279**, 548.
- T. Suominen, P. Uutela, R. A. Ketola, J. Bergquist, L. Hillered, M. Fine, H. Zhang, A. Laakso and R. Kostianinen, *PLoS ONE*, 2013, **8**, e68007.
- A. Shrivastava and V. B. Gupta, *Chron. Young. Sci.*, 2011, **2**, 21.
- G. L. Long and J. D. Winefordner, *Anal. Chem.*, 1983, **55**, 712.
- V. Januzaj, V. Mula, G. L. Turdean and L. M. Muresan, *Acta Chim. Slov.*, 2015, **62**, 1.
- H. Xiong, Y. Zhang, S. Wang, K. Liew and J. Li, *J. Phys. Chem. C*, 2008, **112**, 9706.
- H. Li, R. Wang, Q. Hong, L. Chen, Z. Zhong, Y. Koltypin, J. Calderon-Moreno and A. Gedanken, *Langmuir*, 2004, **20**, 8352.
- K. V. R. Chary and C. S. Srikanth, *Catal. Lett.*, 2009, **128**, 164.
- H. He, X. Peng, M. Huang, G. Chang, X. Zhang and S. Wang, *Analyst*, 2014, **139**, 5482.
- S. Rojas, E. Quartapelle-Procopio, F. J. Carmona, M. A. Romero, J. A. R. Navarro and E. Barea, *J. Mater. Chem. B*, 2014, **2**, 2473.
- H. Li, F. Liu, S. Sun, J. Wang, Z. Li, D. Mu, B. Qiao and X. Peng, *J. Mater. Chem. B*, 2013, **1**, 4146.

Journal Name

58. Z. H. He, Y. H. Song, L. Wang, L. L. Wan, H. Z. Zhu and S. Gao, *Asian J. Chem.*, 2012, **24**, 3837.
59. S. Wu, H. Zhao, H. Ju, C. Shi and J. Zhao, *Electrochem. Commun.* 2006, **258**, 2788.
60. A. K. M. Kafi, G. Wu and A. Chen, *Biosens. Bioelectron.*, 2008, **24**, 566.
61. Y. Wang, X. Ma, Y. Wen, Y. Xing, Z. Zhang and H. Yang, *Biosens. Bioelectron.*, 2010, **25**, 2442.
62. H. Zhou, Q. A. Zhang, Y. Qiao, L. Zhang, S. Y. Wu, J. W. Xu and X. M. Song, *Electroanal.*, 2011, **23**, 900.
63. S. Liu and A. Chen, *Langmuir*, 2005, **21**, 8955.
64. M. Liu, S. He and W. Chen, *Nanoscale*, 2014, **6**, 11769.